12

The pH Dependence of Protonation States of Polar Amino Acid Residues Determined by Neutron Diffraction

Nobuo Niimura
Frontier Research Center for Applied Atomic Sciences, Ibaraki University, Shirakata Japan

1. Introduction

The charges of various amino-acid side chains depend on the pH. For example, at a high pH (low acidity conditions), carboxylic acids tend to be negatively charged (deprotonated), and amines tend to be uncharged (unprotonated). At a low pH (high acidity), the opposite is true. The pH at which exactly half of any ionized amino acid is charged in solution is called the pK_a of that amino acid. These pK_a values of such ionizable amino-acid side chains are tabulated in standard textbooks. However, the protonation state of a given amino-acid side chain in a protein cannot be estimated from standard pK_a values measured from isolated amino acids in solution, because inside a protein it may vary significantly depending on the local environment. The electrically charged states of the amino-acid residues are very important in understanding the physiological function of the protein, the interaction between ligands and proteins, molecular recognition, structural stability, and so on.

Neutron Protein Crystallography (NPC) is the unique method to provide the definite protonation states of the amino acid residue in proteins because neutron can identify not only hydrogen atoms but also protons. (N.Niimura et al. 2004,2006, N.Niimura & R. Bau 2008, N.Niimura & A. Podjarny 2011)

Consider one example: Figure 1 shows a typical example of the different protonation states of histidines in met-myoglobin at pH 6.8. To create this figure, the Neutron Protein Crystallography (NPC) of met-myoglobin was carried out at 1.5 Å resolution (A. Ostermann et al. 2005). Met-myoglobin contains 12 histidines. The measured pK_a value of the histidine amino acid in aqueous solution is about 6.0, so the histidines should be neutral at pH 6.8 aqueous solution. However, four kinds of ionization states are observed by NPC in the imidazole ring of histidines as shown in Figure 1. Two histidines are doubly protonated on both $N^{\delta 1}$ and $N^{\varepsilon 2}$ (in red in Figure 1, with an average B-factors of 14.9 Å^2), three are singly protonated (neutral) on $N^{\delta 1}$ (in yellow, with an average B-factors of 4.5 Å^2), and four are singly protonated (neutral) on $N^{\varepsilon 2}$ (in blue, with an average B-factors of 16.5 Å^2). In the three remaining histidines, the protonation state is not clear because of the disordered state of deuterium atoms, the B-factors of which are rather large (in pink in Figure 1, with an average B-factor of 22.9 Å^2). Clearly, histidines inside the protein do not always follow the pK_a value in solution.

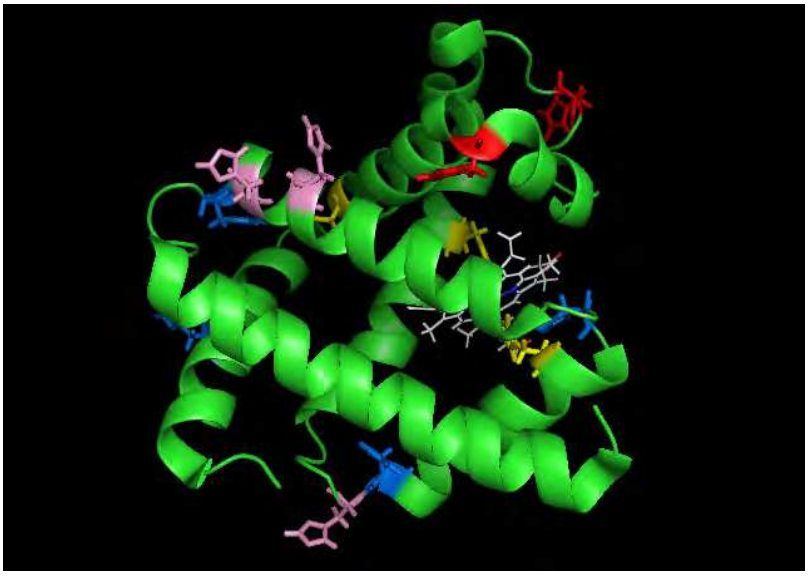

Fig. 1. Protonation states of 12 Histidines in myoglobin.

2. The protonation state of the N^{δ} and N^{ε} atoms of histidine.

2.1 Cubic insulin

Insulin is a polypeptide hormone critical for the metabolism of glucose. The insulin monomer consists of two chains—a 21-residue A-chain and a 30-residue B-chain—linked by a pair of disulfide bonds, A7-B7 and A20-B19, respectively; furthermore, an additional intra-chain disulfide bond links A6 and A11. In a solution free of metal ions, insulin exists as a mixture of monomer, dimer, tetramer, hexamer, and higher aggregates depending on its concentration (T. Blundell et al. 1972). The structure of hexameric insulin, the form in which it is stored in the pancreas β-cells, was reported first in 1969 (Adams et al. 1969); and a comprehensive description of the room-temperature structure at 1.5 Å resolution, as well as the biological implications thereof, was published afterwards (Baker et al. 1988). The structure of the insulin monomer, which is the hormonally active form, was determined by NMR (T. L. Blundell et al. 1971; T. Blundell et al. 1972). Zn^{2+} ions promote the hexamerization of insulin in pancreas, and the other divalent cations, such as Ni^{2+}, Co^{2+}, Cd^{2+} and Cu^{2+}, also have the same effect for the hexamerization in solution (Hill et al. 1991).

Normally, the standard pK_a value of histidine is about 6.0. In insulin, there are two histidine amino acid residues (both on chain B); and it is of interest to know whether at pD 6.6 (pD is the pH in heavy water.) they are protonated or deprotonated, since pD 6.6 is clearly close to the borderline pK_a value. Moreover, it is also important to know which of the two nitrogen atoms (N^{δ}, N^{ε}) in the imidazole ring of histidine are ionized, in order to discuss the physiological function of insulin. (In fact, His *B*10 is a zinc-ion binding site.) (Ishikawa et al. 2008a; Ishikawa et al. 2008b) X-ray structural studies of insulin at various pH values reported that a conformational change of His *B*10 is likely to occur at pH values higher (i.e., more basic) than pH 9, but that of His *B*5 is expected to be unchanged (Diao 2003).

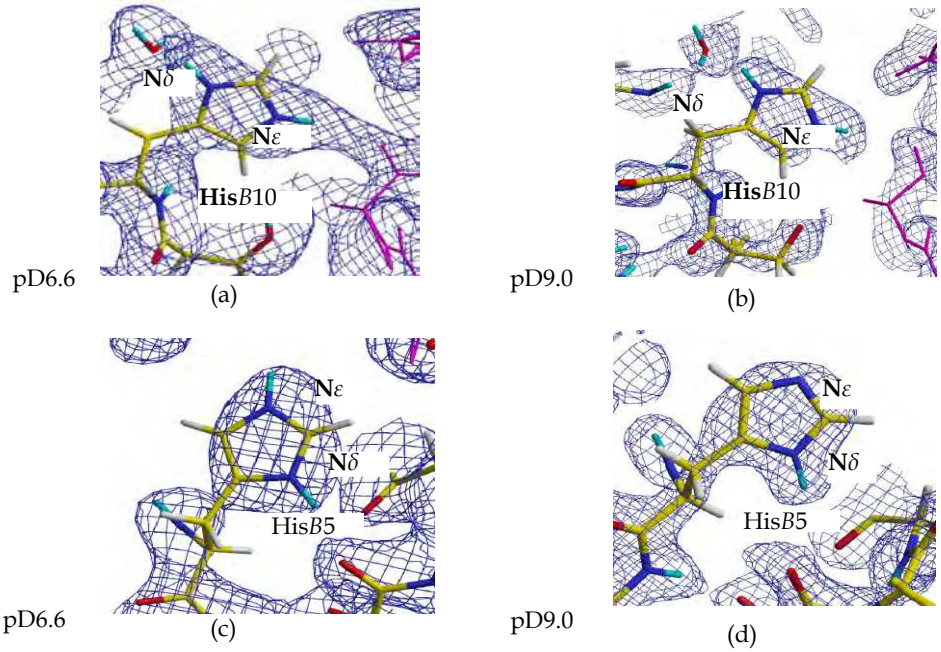

Fig. 2. 2Fo-Fc positive nuclear density maps in insulin of (a) His *B*10 at pD 6.6, (b) His *B*10 at pD 9.0, (c) His *B*5 at pD 6.6, and (d) His *B*5 at pD 9.0.

Porcine insulin can crystallize in a cubic space group without zinc, and neutron diffraction experiments on porcine insulin (crystallized at pD 9.0 and 6.6) were performed at room temperature (Ishikawa et al. 2008a; Maeda et al. 2004). The overall root-mean-square differences of non-hydrogen atoms and all atoms between pD6.6 (Adams et al. 1969) and pD9 are 0.67 Å^2 and 1.04 Å^2, respectively. Porcine insulin has two histidines (HisB5 and HisB10) in the B chain. As for HisB5, both of N$^\delta$ and N$^\varepsilon$ atom of the imidazole ring are protonated at pD6.6, and only the N$^\varepsilon$ atom was protonated at pD9 (Figure 2 (c) and (d)). This fact indicates that the pK_a value of HisB5 has the range between pD6.6 and pD9, which is plausible because of the pK_a value (=6.5) of a simple histidine moiety. However, HisB10 was confirmed to be protonated at both the N$^\delta$ and N$^\varepsilon$ atoms at both pDs. (See Figure 2 (a) and (b)). Figure 2 (b) shows that HisB10 is doubly protonated and positively charged even at the alkaline pD of 9.0. There are two possible reasons for this double-protonation state; a hydrogen bonding network and an electrostatic potential. In HisB10, two D atoms of the imidazole ring are anchored to the surrounding water molecules and amino acids by hydrogen bonds. At both pD6.6 and pD9, the N$^\varepsilon$-D group was hydrogen bonded to a carbonyl group of the main chain of TyrA14. (The δD-O bond lengths were 2.3 Å and 2.1 Å for pD9 and pD6.6, respectively.) At the same time, the N$^\delta$-D group formed an indirect interaction with a carbonyl group of HisB5 mediated by a water molecule. Moreover, HisB10 is located on the surface of insulin and near a negative electrostatic potential. GluB13 was about 7 Å away from HisB10 and the carboxyl group of this residue was deprotonated, indicating negatively charged states of this functional group. In order to investigate the

electrostatic effect for HisB10, molecular surfaces and electrostatic grid potentials were calculated by GRASP2 (Diao 2003). HisB10 was not on a negative potential surface; however, the negative potential derived from GluB13 was in the vicinity of the imidazole ring of HisB10. On the other hand, there was no negative potential near HisB5, which has a normal pK_a value. In the previous X-ray study, it was reported that GluB13 affected a structural change of insulin by pH shift, supporting the hypothesis in the neutron study (Diao 2003). These hydrogen bonds and electrostatic potentials seem to stabilize the double protonation state of HisB10.

The abnormal pK_a value of HisB10 higher than 9.0 indicates the high affinity for positive ions. This property would be effective to the polymerization of insulin depending on various cations. HisB10 captured the D^+ atom instead of the divalent metal cation in the absence of Zn^{2+} ion. This structure would be the active form of insulin at biological pH levels. This mechanism would be achieved by the cation capturing of HisB10; therefore, HisB10 is essential for polymerization of insulin in organisms.

2.2 2Zn Insulin

In the case of the hexamer state, the crystal asymmetric unit contains two insulin monomers (a dimer) related by a pseudo-two-fold axis as shown in; the crystallographic three-fold axis generates the insulin hexamer from three dimers, as shown in Figure 3. (Two zinc ions, on opposite sides of the hexamer, are situated on the crystallographic three-fold axis; each is octahedrally coordinated by the three crystallographically related HisB10 $N^{\varepsilon 2}$ atoms and three water molecules. The coordination of metal ions is intrinsically the problem of protonation/deprotonation of the polar amino acid residues, and only NPC can reveal the protonation states.

To understand the octahedrally coordinated structure of the zinc ions and the coordination mechanism thereof, it is essential to know the protonation and/or deprotonation states of not only HisB10 $N^{\varepsilon 2}$ but also HisB10 $N^{\delta 1}$. In the hexamer insulin crystals, three dimers are assembled around two zinc ions (upper Zn (u) and lower Zn (l)), 16.4 Å apart on the three-fold axis. Parts (a) and (b) of Figure 4 show (2*Fo*-*Fc*) maps of the areas around upper Zn (u) and lower Zn (l), respectively. The $N^{\varepsilon 2}$ atom of HisB10 is deprotonated and coordinated to Zn, whereas $N^{\delta 1}$ of HisB10 is protonated, making the net charge of HisB10 neutral. The two molecules in the dimer are designated molecule 1 and molecule 2, as shown in Figure 3 (a) and (b). Residues belonging to either molecule 1 or molecule 2 are distinguished by the suffix .1 or .2 after the residue number. Thus, the upper zinc is coordinated to three symmetry-related $N^{\varepsilon 2}$ atoms of HisB10.1 (i.e., from molecule 1) and three water molecules, while the lower Zn is coordinated to the three symmetry-related $N^{\varepsilon 2}$ atoms of HisB10.2 and three water molecules, as shown in Figure 4 (a) and (b), respectively. (Iwai et al. 2009) From the top, three water molecules can be seen coordinating the upper Zn (u) and from the bottom, another three water molecules can be seen coordinating the lower Zn (l). The Former three water molecules are classified as triangular, since the deuterium atoms of these water molecules could be placed. On the other hand, the latter three water molecules are classified as stick-shaped and are presumably rotating about OD axis. These facts are well supported by the B-factors, which are smaller for the triangular molecules (36.5 $Å^2$) than for the ball-shaped ones (74.0 $Å^2$) (Chatake et al. 2003). Differences in the dynamic behavior of the coordinated water molecules, between the upper and lower Zn ions, can be observed in

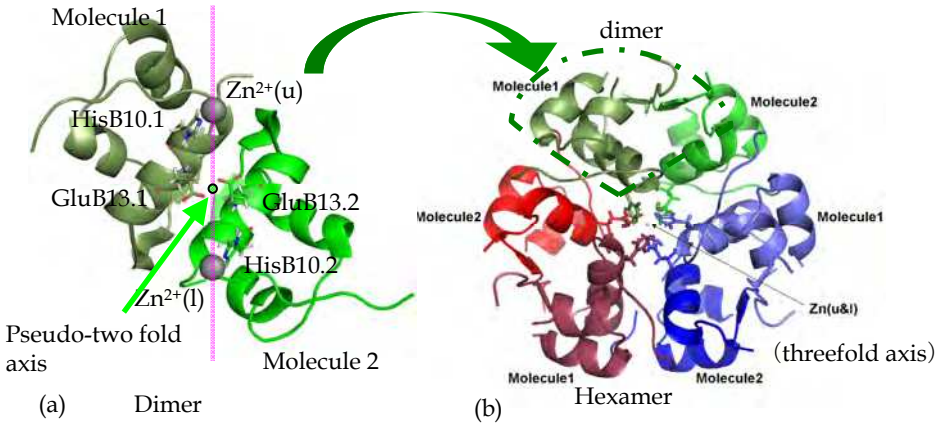

Fig. 3. (a) Model of the crystal asymmetric unit showing two insulin monomers (a dimer) related by a pseudo-two-fold axis. (b) Model of the insulin hexamer from three dimers generated by the crystallographic three-fold axis.

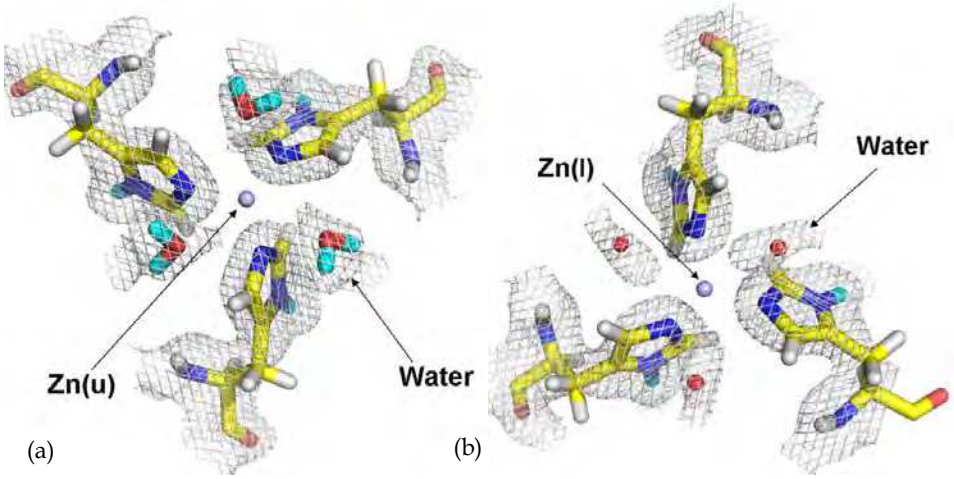

Fig. 4. 2Fo-Fc maps of the areas around upper Zn (u) and lower Zn (l) of insulin.

the structure of hexamer human insulin at 1.0 Å resolution, at 120 K, in which the unambiguous electron density of three water molecules coordinating the upper Zn ion was observed (Smith and Blessing 2003). Continuous electron density for the three water molecules coordinating the lower Zn ion can also be observed, suggesting that it would be possible for a disordered anion—such as a citrate—to occupy this site (Smith et al 2003). Furthermore, in the structure of a dried crystal of hexamer human insulin at 100 K, the upper Zn ion binds three water molecules and adopts an octahedral coordination in the crystal, whereas the lower zinc ion adopts a tetrahedral coordination, with the three water molecules being replaced by a single chloride ion (Smith et al. 2003).

In the neutron crystallography results, a difference in the temperature factor of $N^{\varepsilon 2}$ of HisB10 coordinating with Zn ions was also observed: The temperature factors were 9.3 $Å^2$ for $N^{\varepsilon 2}$ of HisB10.1 coordinating the upper Zn ion and 14.6 $Å^2$ for $N^{\varepsilon 2}$ of HisB10.2 coordinating the lower Zn ion.

2.3 RNase A

Bovine pancreatic ribonuclease A (RNase A) is a major ribonuclease in the bovine pancreas, which cleaves and hydrolyzes RNA exclusively at pyrimidine nucleotide positions. RNase A consists of 124 amino acids, has a mass of about 14 kDa and an isoelectric point of pH 9.6, and is a comparatively stable protein. The structure was initially solved by X-ray diffraction analysis at 5.5 Å resolution (Avey et al. 1967). Subsequently, a high resolution (1.05 Å) X-ray diffraction analysis of RNase A was carried out at six different pH values (Berisio et al. 2002).

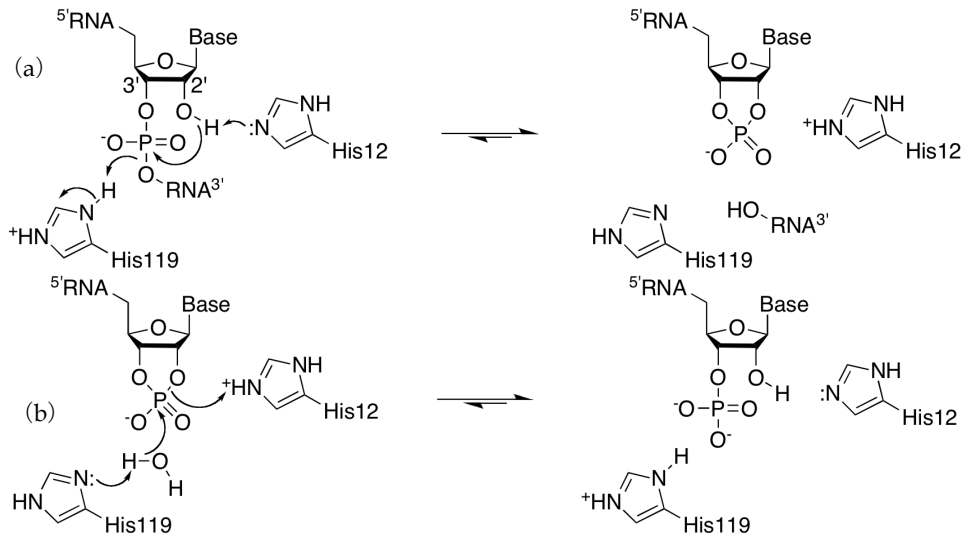

Fig. 5. Putative mechanism of catalysis by ribonuclease A. (a) Transphosphorylation reactions. (b) Hydrolysis reaction. (As taken from ref: Park, C., Schultz, L. W., Raines, R. T. (2001) Contribution of the active site histidine residues of ribonuclease A to nucleic acid binding, Biochemistry 40, 4949-4956.)

Two histidine residues, His12 and His119, play a key role in the cleavage reaction catalyzed by RNase A (Findlay et al. 1962; C. Park et al. 2001; Wlodawer 1980). In this transphosphorylation reaction, His12 acts as a base to abstract a proton from the 2′-hydroxyl group of a ribose ring, while His119 acts as an acid to donate a proton to the 5′-oxygen of the leaving group (Figure 5 (a)). The roles of His12 and His119 as base and acid are switched in the subsequent hydrolysis reaction of 2′,3′-cyclic nucleotide substrates (Figure 5 (b)). It is important to know the protonation states of His12 and His119 to understand the hydrolysis mechanism of ribonuclease A. Neutron protein crystallography can therefore contribute significantly to the understanding of this catalytic mechanism.

The structure of the active site of phosphate-free RNase A was determined by a neutron diffraction experiment (Yagi et al. 2009). In the phosphate-bound model (Figure 6 (a)), O^1 of the phosphate (PO_4) group is hydrogen-bonded to the $D^{\delta 1}$ of His119 and O^2 of the phosphate group is hydrogen-bonded to the $D^{\varepsilon 2}$ of His12. In the phosphate-free model, the PO_4 group is replaced by three water molecules (Wlodawer et al. 1986), DOD41, DOD76, and O89, as shown in Figure 6 (b), and the H-bonds occur now with these water molecules. The oxygen of DOD41 is hydrogen-bonded to the $D^{\varepsilon 2}$ atom of His12. The $D^{\delta 1}$ atom of His119 is hydrogen bonded to the oxygen of O89 (2.3 Å), while the $D^{\varepsilon 2}$ atom of His119 is hydrogen-bonded to the $O^{\delta 1}$ atom of Asp121. It was reported that at pH 6.3, the active site has a sulphate ion, which is hydrogen bonded to the ordered His119, whereas at pH 7.1 the active site releases the sulphate ion and has a disordered His119 (Berisio et al. 2002). Although a soaking solution at pD 6.2 was used in this study, the active site does not have the sulphate group, and His119 is ordered. (DOD37 and DOD39 occupy the place of the alternative conformation of His119.) This difference might come from two different crystallization methods. The oxygen of DOD41 forms possible hydrogen bonds with D^2 of DOD37, D^1 of DOD3, and O of DOD76. DOD3 is hydrogen-bonded to the $D^{\varepsilon 2}$ of Gln11. DOD3 is one of the most deeply buried water molecules in the pocket of the catalytic site and has a B-factor of 17.1 $Å^2$, which is lower than those of other water molecules located at the surface of RNase A. The B-factor of DOD41 is 42.1 $Å^2$, which is higher than those of other water molecules, the average value of which is 29.2 $Å^2$. This fact suggests that DOD41 could be relatively easily replaced by other substrates. The occupancy of DOD41 may also be affected by the protonation states of His12, a hydrogen-bonding partner.

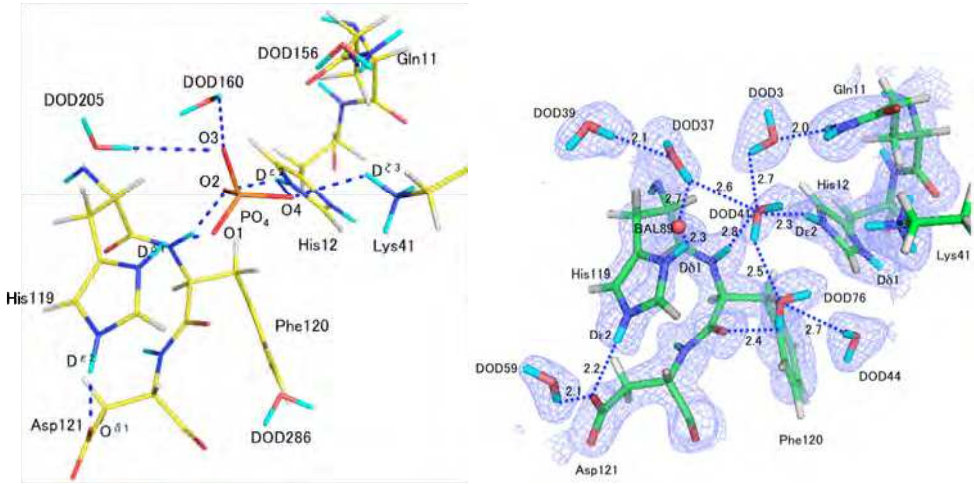

(a) (b)

Fig. 6. The structure of the active site of phosphate-free RNase A determined by a neutron diffraction experiment. (a) The phosphate-bound model. (b) The phosphate-free model (blue contours: positive 2Fo-Fc map).

His12 and His119 are located at the catalytic site of RNase A and play important roles in the process of enzymatic activity (Figure 5). His12 is known to act as a general base that extracts a proton from the RNA 2'-OH group and thereby promotes its nucleophilic attack on the adjacent phosphorus atom. On the other hand, His119 is believed to act as general acid,

enabling bond scission by donating a proton to the leaving group. To act as a base, His12 should be singly protonated. However, double protonation of His12 at acidic pH has been reported from both X-ray and neutron diffraction analyses (Berisio et al. 2002; Wlodawer et al. 1983; Wlodawer et al. 1986). Neutron diffraction analysis suggested at first glance that His12 is doubly-protonated (positively charged) (Usher et al. 1972). If that would be the case, it would be impossible for His12 to extract a proton from the 2′-OH group of RNA under these conditions. To confirm the protonation state of His12, an ($|Fo|-|Fc|$) nuclear density map was calculated after first omitting $D^{\delta 1}$ and $D^{\varepsilon 2}$ of His12, as shown in Figure 7. The nuclear density for $D^{\delta 1}$ is higher than that for $D^{\varepsilon 2}$ at the 5σ level, implying a lower occupancy for $D^{\varepsilon 2}$. This result means that a certain proportion of His12 residues have a singly protonated imidazole ring, allowing the proton from the RNA 2'-OH group to be extracted at pD 6.2. These results support the hypothesis that His12 is singly-protonated part of the time and is capable of acting as a general base in the catalytic mechanism of RNase A.

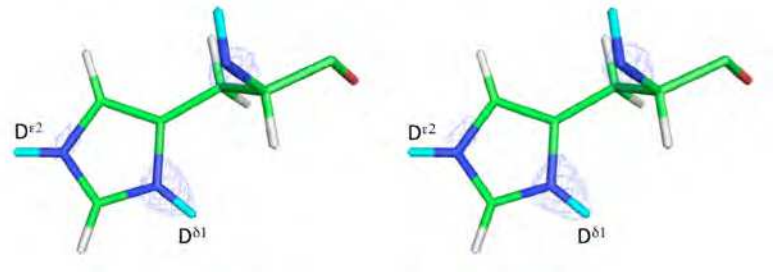

Fig. 7. A stereo view of an omit map showing the His12 residue of RNase A. (Blue contours show positive peaks at 10σ.)

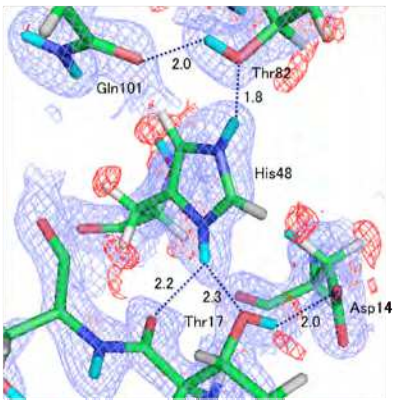

Fig. 8. A 2Fo-Fc nuclear density map around the His48 residue of RNase A.. (Blue contours are at 1.5σ, and red contours are at −2.5σ.) H-bonds are indicated by broken lines. Gln101 is hydrogen bonded from atom donates a hydrogen bond to the carbonyl oxygen atom of the Gln101 side-chain (H...O distance 2.0 Å). The $N^{\delta 1}$ atom of the His48 imidazole acts as a donor in a bifurcated manner, donating a H-bond not only to the $O^{\gamma 1}$ atom of Thr17 (H...$O^{\gamma 1}$ 2.3 Å), but also to its backbone carbonyl oxygen atom (H...O 2.2 Å). Finally, the $O^{\gamma 1}$ hydroxyl group of Thr17 acts as a H-bond donor to the $O^{\delta 2}$ atom of Asp14 (H...$O^{\delta 2}$ 2.0 Å).

The details of the hydrogen bonding network around His48 at various pHs were speculated upon - without knowing the actual positions of the H atoms - in an earlier X-ray analysis. This estimation was done in order to explain the movement of the Gln101 residue at alkaline pH (Berisio et al. 2002). In the neutron diffraction results, this speculation was confirmed not only by determining the H atom positions but also by defining their donor and/or acceptor characteristics (Figure 8)The $N^{\varepsilon 2}$ atom of the His48 imidazole ring donates a hydrogen bond to $O^{\gamma 1}$ of Thr82 (with an H…$O^{\gamma 1}$ distance of 1.8 Å), and the $O^{\gamma 1}$

His48 through the Thr82 residue. Note that this histidine residue is doubly-protonated and that one of the two N-H bonds forms a bifurcated H-bond with two oxygen atoms.

2.4 Trypsin-BPTI complex

The target enzyme of BPTI, bovine trypsin, is a well-known serine protease. This protein is a member of the chymotrypsin family of proteases, and its active residues are His57, Ser195 and Asp102 (based on the numbering of residues in chymotrypsin). The catalytic mechanism of BPTI has been extensively studied, and thus the reaction mechanism of this protease is suggested in many previous reports. Trypsin is specific to basic amino acids—lysine and arginine—and the substrate recognition site is Asp189 (Voet *et al.*, 1999; Hedstrom, 2002; Bode & Huber, 1992).

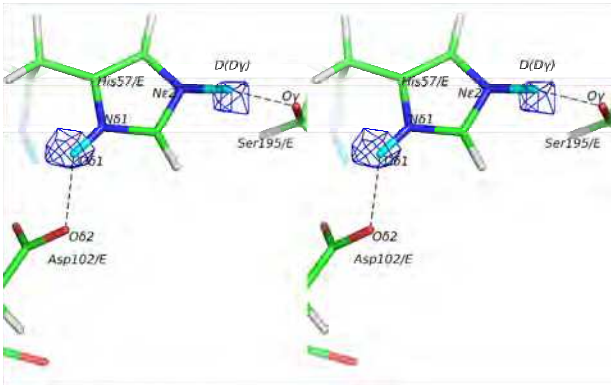

Fig. 9. The F_o-F_c nuclear density maps (in stereo view) of the catalytic triad in the Trypsin-BPTI complex. The maps have been calculated without the $D^{\delta 1}$ and $D(D^{\gamma})$ deuterium atoms and are contoured at 5.5 σ positive density. The broken line indicates a hydrogen bond between the hydrogen atom and the acceptor atom.

The specific roles of the $HisN^{\varepsilon 2}$ within the catalytic triad of serine proteases are as follows: to act as a base and extract the H from the –OH of the hydroxyl group of serine; to act as an acid and transfer H to the scissile peptide amide; to act as a base and extract the H from a hydrolytic H_2O molecule; and to act as an acid and transfer H to the deprotonated $–O^-$ of the hydroxyl group of serine. The protonation state of the $His57N^{\varepsilon 2}$ is crucial to understanding the catalytic mechanism of trypsin, because the $N^{\varepsilon 2}$ serves as both a base and an acid for activating the nucleophilic species of Ser195 and for transferring a proton to the leaving group-NH in the substrate polypeptide, respectively. In this study, we used neutron crystal-structure analysis to examine the protonation (deuteration) states of the catalytic triad (Asp102, His57 and Ser195 of

trypsin) of trypsin in the complex state with BPTI, which is in a Michaelis complex state. Figure 9 shows the F_o-F_c nuclear-scattering map of both His57D$^{\delta 1}$ and Ser195D$^{\gamma}$ in the trypsin–BPTI complex (Kawamura et al. 2011); this map was made at the 5.5σ contour level and was calculated without incorporation of the D atoms. Using this method, we found two positive peaks, with one between Asp102O$^{\delta 2}$ and His57N$^{\delta 1}$ and the other between His57N$^{\varepsilon 2}$ and Ser195O$^{\gamma}$. The distances between Asp102O$^{\delta 2}$ and D$^{\delta 1}$ and between D$^{\delta 1}$ and His57N$^{\delta 1}$ were determined to be 2.0 Å and 1.0 Å, respectively. The distance between Asp102O$^{\delta 2}$ and His57N$^{\delta 1}$ was 2.8 Å, and the angle of O$^{\delta 2}$-D$^{\delta 1}$-N$^{\delta 1}$ was ~140°.The distances between His57N$^{\varepsilon 2}$ and D$^{\gamma}$ and between D$^{\gamma}$ and Ser195O$^{\gamma}$ were determined to be 1.3 Å and 1.7 Å, respectively. The distance between His57N$^{\varepsilon 2}$ and Ser195O$^{\gamma}$ was 2.8 Å, and the angle of N$^{\varepsilon 2}$-D$^{\gamma}$-O$^{\gamma}$ was ~144°.

3. Carboxylate groups of acidic residues

3.1 Lysozyme

The enzymatic activity of lysozyme, a saccharide-cleaving enzyme, is maximal at pH 5 and diminishes at pH 8. It has been postulated that, at pH 5, the carboxyl group of Glu35 is protonated and that it is this proton that is transferred to the oxygen atom of the bound substrate (an oligosaccharide) during the hydrolysis process. During the reaction, another acidic residue, Asp52, is postulated to remain in its dissociated (anionic) state (D. C. Phillips 1966). To elucidate the role of hydrogen atoms in this reaction, neutron diffraction experiments of hen egg-white lysozyme were carried out, using crystals that were grown at different acidities, specifically, pD = 4.9 on BIX and pD = 8.0 on LADI (Maeda et al. 2001; N. Niimura et al. 1997b; N. Niimura et al. 1997a). The (2|*Fo*|–|*Fc*|) nuclear density maps around the carboxyl group of Glu35 are shown at pD 4.9 in (a) and at pD 8.0 in (b). At pD 4.9, the Fourier map shows a positive region (at the arrow in Figure 10 (a)) extending beyond (i.e., attached to) the position of the O atom of the carboxyl group labeled E35 O$^{\varepsilon 1}$, suggesting that this carboxyl oxygen atom (circled) is protonated at pD 4.9. On the other hand, at pD 8.0, it can be seen that this residue is deprotonated (the circled atom in Figure 10 (b)), and hydrogen-bonded to a water molecule. The observation that the Glu35 catalytic site is deprotonated at pD 8.0 rationalizes why lysozyme has significantly reduced activity at neutral conditions. Thus, these results suggest that Glu35 is the site of the enzymatically active proton that is subsequently transferred to the oxygen atom of the carbohydrate substrate during the hydrolysis process. Incidentally, these results at the less acidic pH value of 8.0 (N. Niimura et al. 1997a) are consistent with the conclusions of an earlier neutron investigation, as described in a paper by Mason and co-workers many years ago (Mason et al. 1984).

4. How to grow a large single crystal under different pH

One of the highest barriers of neutron protein crystallography experiments is the supply of large single crystals. Single crystals larger than 1mm^3 at least are necessary for neutron diffraction experiments because of the weak incident neutron beams so far. The crystallization phase diagram is very helpful to grow a large single crystal. The crystallization of HEWL at wide range of pH from 2.5 to 8.0 with 0.5 step was carried out as follows: HEWL was crystallized in a buffer of 50 mM NaH_2PO_4, 33.5 mg/ml protein concentration, 3.5 w/v% NaCl as the crystallization agent and T= 20°C at each pH by batch method. The condition is indicated by a yellow filled circle in the crystallization phase diagram as shown in Figure 11 and this condition was fixed in the following preliminary crystallization experiment at wide range of pH (Iwai et al. 2008). The pHs of solutions at pH

2.5 - 4.5 and at pH 5.0 - 8.0 were adjusted in 50 mM NaH_2PO_4 buffer with H_3PO_4 and with Na_2HPO_4, respectively, in order to prepare solutions of wide range of pH. Crystallization at pH 2.5 - 6.5 was carried out in the designed pH solution directly. Crystals did not appear beyond pH 7.0 and therefore the crystals at pH 7.0 - 8.0 were prepared by soaking crystals (initially grown at pH 5.5) in the solution of designed pH in the meta-stable region. Crystallization phase diagrams at pH 2.5, 6.0, 7.5 were determined. (Figure 12) At pH less than 4.5 the border between meta-stable region and nucleation region shifted to the left (lower precipitant concentration) and at larger than 4.5 the border shifted to the right (higher precipitant concentration) in the phase diagram. The qualities of these crystals were characterized by Wilson plot method.(Arai et al. 2002) The qualities of all crystals at different pH were more or less equivalent (B-factor values are within 25 - 40). It is expected that the neutron diffraction from these crystals of different pH provides equivalent data in quality for discussion of protein pH titration in the crystalline state of HEWL.

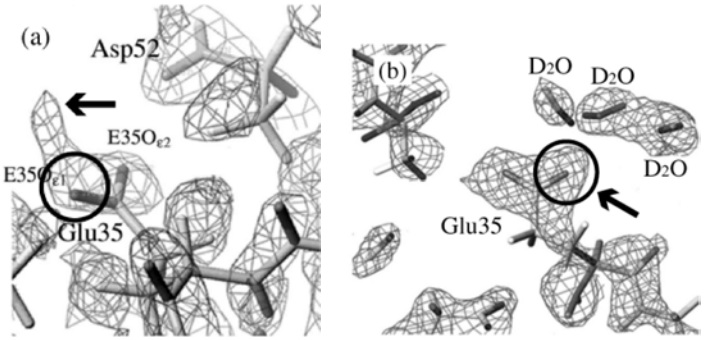

Fig. 10. The 2 Fo–Fc nuclear density maps around the carboxyl group of Glu35 of HEWL (a) at pD 4.9 and (b) at pD 8.0. The Fourier map at pD 4.9 shows a positive region extending beyond (i.e., attached to) the position of the O atom of the carboxyl group labeled E35 Oε1.

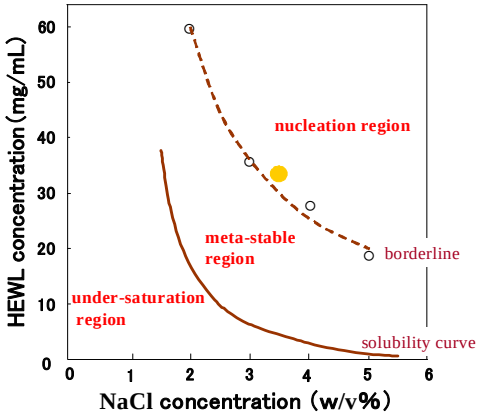

Fig. 11. Crystallization phase diagram of HEWL at pH 4.5 and at 20°C. The plots of circles (o) are experimental data. A solid line is solubility curve and a broken line is a borderline, guide for eyes respectively.

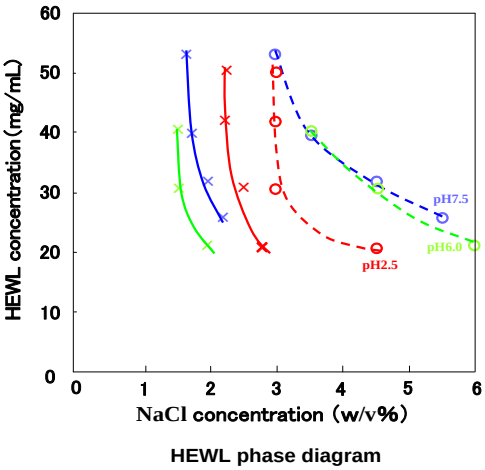

Fig. 12. The results of crystallization phase diagrams of HEWL at 20°C. The cross (x) and circle (o) are experimental data. Solid lines are solubility curves and broken lines are borderlines, guide for eyes respectively. Results at pH 2.5, 6.0 and 7.5 are drawn in red, green and blue, respectively.

5. Conclusion

The determination of protonation states has historically been a major application of neutron diffraction. Biological mechanism such as enzymatic reactions depend on these protonation states, but they cannot always be obtained from X-ray diffraction data. On the other hand, since neutrons scatter from nucleus in proteins, neutron interacts with protons and identify the protonation states in proteins. These were certificated by several examples, such as insulin, RNase A, Trypsin-BPTI complex and lysozyme.

One of the most difficult probles in NPC is to obtain a single crystal that is large enough to obtain diffraction results with the low flux of a neutron beam. Often, a crystal with a volume of several cubic millimeters is required. To grow such a large single crystal of a proein, a seed crystal is placed into a metastable growth environment, in which new crystals do not nucleate but protein molecules stillcrystallize on the seed crystal. This method was demonstrated successfully in case of the crystallization of lysozyme under different pH.

6. References

Adams, M. J., et al. (1969), 'Structure of Rhombohedral 2 Zinc Insulin Crystals', *Nature,* 224 (5218), 491-95.

Arai, S., et al. (2002), 'Crystallization of a large single crystal of a B-DNA decamer for a neutron diffraction experiment by the phase-diagram technique', *Acta Crystallogr D Biol Crystallogr,* 58 (Pt 1), 151-3.

Avey, H. P., et al. (1967), 'Structure of ribonuclease', *Nature,* 213 (5076), 557-62.

Baker, E. N., et al. (1988), 'The structure of 2Zn pig insulin crystals at 1.5 A resolution', *Philos Trans R Soc Lond B Biol Sci,* 319 (1195), 369-456.

Berisio, R., et al. (2002), 'Atomic resolution structures of ribonuclease A at six pH values', *Acta Crystallogr D Biol Crystallogr,* 58 (Pt 3), 441-50.

Blundell, Tom, et al. (1972), 'Insulin: The Structure in the Crystal and its Reflection in Chemistry and Biology by', in Jr John T. Edsall C.B. Anfinsen and M. Richards Frederic (eds.), *Advances in Protein Chemistry* (Volume 26: Academic Press), 279-86, 86a, 87-402.

Blundell, T. L., et al. (1971), 'X-ray analysis and the structure of insulin', *Recent Prog Horm Res,* 27, 1-40.

Bode, W. & Huber, R. (1992). 'Natural protein proteinase inhibitors and their interaction with proteinases.' *Eur J Biochem.* 204, 433–451.

Chatake, T., et al. (2003), 'Hydration in proteins observed by high-resolution neutron crystallography', *Proteins,* 50 (3), 516-23.

Diao, J. (2003), 'Crystallographic titration of cubic insulin crystals: pH affects GluB13 switching and sulfate binding', *Acta Crystallogr D Biol Crystallogr,* 59 (Pt 4), 670-6.

Findlay, D., et al. (1962), 'The active site and mechanism of action of bovine pancreatic ribonuclease. 7. The catalytic mechanism', *Biochem J,* 85 (1), 152-3.

Hedstrom, L. (2002). 'Serine protease mechanism and specificity', *Chem Rev.* 102, 4501–4524.

Hill, C. P., et al. (1991), 'X-ray structure of an unusual Ca2+ site and the roles of Zn2+ and Ca2+ in the assembly, stability, and storage of the insulin hexamer', *Biochemistry,* 30 (4), 917-24.

Ishikawa, Takuya, et al. (2008a), 'An abnormal pKa value of internal histidine of the insulin molecule revealed by neutron crystallographic analysis', *Biochemical and Biophysical Research Communications,* 376 (1), 32-35.

--- (2008b), 'A neutron crystallographic analysis of a cubic porcine insulin at pD 6.6', *Chemical Physics,* 345 (2-3), 152-58.

Iwai, W., et al. (2008) 'Crystallization and evaluation of Hen Egg-White Lysozyme (HEWL) crystals for protein pH titration in the crystalline state.', *J. Synchr. Rad.* , 58, 312-315

Iwai, W., et al. (2009), 'A neutron crystallographic analysis of T6 porcine insulin at 2.1 A resolution', *Acta Crystallogr D Biol Crystallogr,* 65 (Pt 10), 1042-50.

Kawamura,K. , et al: (2011) 'X-ray and neutron protein crystallographic analysis of the trypsin-BPTI complex', *Acta Crystallogr D Biol Crystallogr,* 67, 140-148

Maeda, M., et al. (2001), 'Neutron structure analysis of Hen Egg-White Lysozyme at pH 4.9', *J. Phys. Soc. Jpn. Suppl. A,* 70, 403-05.

Maeda, M., et al. (2001), 'Neutron structure analysis of Hen Egg-White Lysozyme at pH 4.9', *J. Phys. Soc. Jpn. Suppl. A,* 70, 403-05.

--- (2004), 'Crystallization of a large single crystal of cubic insulin for neutron protein crystallography', *J Synchrotron Radiat,* 11 (Pt 1), 41-4.

Mason, S. A., Bentley, G. A., and McIntyre, G. J. (1984), 'Deuterium exchange in lysozyme at 1.4-A resolution', *Basic Life Sci,* 27, 323-34.

Niimura, N., et al. (2004), 'Hydrogen and hydration in proteins', *Cell Biochem Biophys,* 40 (3), 351-69.

--- (2006), 'Recent results on hydrogen and hydration in biology studied by neu tron macromolecular crystallography', *Cell Mol Life Sci,* 63 (3), 285-300.

--- (1997a), 'Neutron Laue diffractometry with an imaging plate provides an effective data collection regime for neutron protein crystallography', *Nat Struct Biol,* 4 (11), 909-14.

--- (1997b), 'Neutron Laue diffractometry with an imaging plate provides an effective data collection for neutron protein crystallography', *Physica B: Condensed Matter,* 241-243, 1162-65.

Niimura, N. and Bau, R. (2008), 'Neutron protein crystallography: beyond the folding structure of biological macromolecules', *Acta Crystallogr A,* 64, 12-22.

Niimura,N., & Podjarny, A., (2011) 'Neutron Protein Crystallography. Hydrogen, Protons, and Hydration in Bio-macromolecules.' ISBN 978-0-19-957886-3, Oxford University Press.

Ostermann, A. and Parak, F. G. (2005), 'Hydrogen Atoms and Hydration in Myoglobin: Results from High Resolution Protein Neutron Crystallography', in N. Niimura, et al. (eds.), *Hydrogen- and Hydration-Sensitive Structural Biology* (Tokyo: KubaPro), 87-102.

Park, C., Schultz, L. W., and Raines, R. T. (2001), 'Contribution of the active site histidine residues of ribonuclease A to nucleic acid binding', *Biochemistry,* 40 (16), 4949-56.

Phillips, D. C. (1966), 'The three-dimensional structure of an enzyme molecule', *Sci Am,* 215 (5), 78-90.

Smith, G. D. and Blessing, R. H. (2003), 'Lessons from an aged, dried crystal of T(6) human insulin', *Acta Crystallogr D Biol Crystallogr,* 59 (Pt 8), 1384-94.

Smith, G. D., Pangborn, W. A., and Blessing, R. H. (2003), 'The structure of T6 human insulin at 1.0 A resolution', *Acta Crystallogr D Biol Crystallogr,* 59 (Pt 3), 474-82.

Usher, D. A., Erenrich, E. S., and Eckstein, F. (1972), 'Geometry of the first step in the action of ribonuclease-A (in-line geometry-uridine2',3'-cyclic thiophosphate- 31 P NMR)', *Proc Natl Acad Sci U S A,* 69 (1), 115-8.

Voet, D., Voet, J. G. & Pratt, C. W. (2008). *Fundamentals of Biochemistry*. (3rd Edition.) New York: John Wiley & Sons.

Wlodawer, A. (1980), 'Studies of ribonuclease-A by X-ray and neutron diffraction', *Acta Crystallographica Section B,* 36 (8), 1826-31.

Wlodawer, A., Miller, M., and Sjolin, L. (1983), 'Active site of RNase: neutron diffraction study of a complex with uridine vanadate, a transition-state analog', *Proc Natl Acad Sci U S A,* 80 (12), 3628-31.

Wlodawer, A., et al. (1986), 'Comparison of two independently refined models of ribonuclease-A', *Acta Crystallographica Section B,* 42 (4), 379-87.

Yagi, D., et al. (2009), 'A neutron crystallographic analysis of phosphate-free ribonuclease A at 1.7 A resolution', *Acta Crystallogr D Biol Crystallogr,* 65 (Pt 9), 892-9.

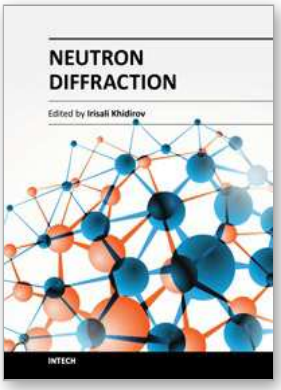

Neutron Diffraction

Edited by Prof. Irisali Khidirov

ISBN 978-953-51-0307-3
Hard cover, 286 pages
Publisher InTech
Published online 14, March, 2012
Published in print edition March, 2012

Now neutron diffraction is widely applied for the research of crystal, magnetic structure and internal stress of crystalline materials of various classes, including nanocrystalls. In the present book, we make practically short excursion to modern state of neutron diffraction researches of crystal materials of various classes. The book contains a helpful information on a modern state of neutron diffraction researches of crystals for the broad specialists interested in studying crystals and purposeful regulation of their service characteristics, since the crystal structure, basically, defines their physical and mechanical properties. Some chapters of the book have methodical character that can be useful to scientists, interested in possibilities of neutron diffraction. We hope, that results of last years presented in the book, can be a push to new ideas in studying of crystalline, magnetic structure and a macrostructure of usual crystal materials and nanocrystals. In turn, it can promote working out of new materials with new improved service characteristics and to origin of innovative ideas.

InTech Europe
University Campus STeP Ri
Slavka Krautzeka 83/A
51000 Rijeka, Croatia
Phone: +385 (51) 770 447
Fax: +385 (51) 686 166
www.intechopen.com

InTech China
Unit 405, Office Block, Hotel Equatorial Shanghai
No.65, Yan An Road (West), Shanghai, 200040, China
中国上海市延安西路65号上海国际贵都大饭店办公楼405单元
Phone: +86-21-62489820
Fax: +86-21-62489821